

# Transition Region Emission and Energy Input to Thermal Plasma During the Impulsive Phase of Solar Flares

John C. Raymond

*Harvard-Smithsonian Center for Astrophysics, 60 Garden St., Cambridge, MA 02138*

Gordon Holman

*NASA's GSFC, Code 612.1, Greenbelt, MD 20771*

A. Ciaravella

*INAF-Osservatorio Astronomico di Palermo, P.za Parlamento 1, 90134, Palermo, Italy*

A. Panasyuk, Y.-K. Ko, and J. Kohl

*Harvard-Smithsonian Center for Astrophysics, 60 Garden St., Cambridge, MA 02138*

## ABSTRACT

The energy released in a solar flare is partitioned between thermal and non-thermal particle energy and lost to thermal conduction and radiation over a broad range of wavelengths. It is difficult to determine the conductive losses and the energy radiated at transition region temperatures during the impulsive phases of flares. We use UVCS measurements of O VI photons produced by 5 flares and subsequently scattered by O VI ions in the corona to determine the  $5.0 \leq \log T \leq 6.0$  transition region luminosities. We compare them with the rates of increase of thermal energy and the conductive losses deduced from RHESSI and GOES X-ray data using areas from RHESSI images to estimate the loop volumes, cross-sectional areas and scale lengths. The transition region luminosities during the impulsive phase exceed the X-ray luminosities for the first few minutes, but they are smaller than the rates of increase of thermal energy unless the filling factor of the X-ray emitting gas is  $\sim 0.01$ . The estimated conductive losses from the hot gas are too large to be balanced by radiative losses or heating of evaporated plasma, and we conclude that the area of the flare magnetic flux tubes is much smaller than the effective area measured by RHESSI during this phase of the flares. For the 2002 July 23 flare, the energy deposited by non-thermal particles exceeds the X-ray and UV energy losses and the rate of increase of the thermal energy.

*Subject headings:* Sun: flares – Sun: UV Radiation

## 1. Introduction

The energy released in solar flares appears in a variety of forms, including electromagnetic radiation, energetic electrons and ions, heated plasma, and mass motions ranging from local turbulence to coronal mass ejections (CMEs). To understand the physical mechanisms responsible for this energy release and transport we need to know how energy is partitioned among these channels. Therefore, evaluating the energy contained in these various components is an important part of solar flare research (e. g., Emslie et al. 2004).

A significant fraction of the energy released in moderate to large flares appears as hot plasma with a temperature on the order of 10 to 40 million degrees. X-ray observations of the bremsstrahlung spectrum of this plasma provide temperatures and emission measures which, along with estimates of the plasma volume, allow the energy content of the plasma to be computed. In large flares the maximum value of this thermal energy content is typically found to be comparable to but less than the computed accumulated energy in nonthermal electrons (Holman et al. 2003, Emslie et al. 2004).

Despite substantial progress in our ability to determine these energies, there are still significant uncertainties (e. g., Emslie et al. 2005). For the thermal energy content, one of these is energy losses. Based on numerical simulations of flare loops, Isobe, Takasaki & Shibata (2005) estimate radiative losses at 40% of the energy deposited. On the observational side, Kane, Frost & Donnelly (1979) found a close relationship between EUV and hard X-ray intensities during the impulsive phases of flares, and full-disk spectral observations of a few flares with the SORCE and TIMED satellites (Brekke et al. 1996; Woods et al. 2004) show EUV brightenings that imply significant emission at transition region temperatures. RHESSI observations of the positron annihilation line indicate that much of the annihilation occurred at temperatures of 2 to  $7 \times 10^5$  K and densities above  $10^{13} \text{ cm}^{-3}$  during the impulsive phase of at least one flare (Share et al. 2003, 2004), implying large emission measures and radiation losses at transition region temperatures. To the extent that such energy losses are significant, the energy required to heat the plasma is greater than the computed instantaneous energy content.

Bremsstrahlung losses are easily measured, but thermal conduction of heat into the transition region and related losses are more difficult to determine. Conduction losses are often estimated with the assumption of classical conduction (Spitzer conductivity), taking the conduction scale length to be the flare loop half length (e. g., Veronig et al. 2005). However, the conductivity may not be classical and this scale length may not be correct. In determining the total energy devoted to heating plasma, it is also possible that cooler plasma not observable in X-rays is directly heated by energetic particles. Therefore, the best approach would be to observe the flare plasma in all temperature regimes. This is generally not possible, however.

The development of a large solar flare typically occurs in two parts; the impulsive and gradual phases. The former is attributed to the rapid acceleration of particles, which then deposit their energy in the chromosphere and produce hard X-rays. The latter is associated

with the softer, longer lasting X-ray emission from gas evaporated into the corona. Because the impulsive phase occurs in a small region and only lasts a short time, a spectrograph making raster scans over an active region is unlikely to catch the impulsive phase. Therefore, most spectroscopic observations of flares pertain to the gradual phase.

In view of the above discussion, it is important to constrain the amount of plasma at transition region temperatures in the impulsive phase of flares in order to assess where energy is deposited and to constrain the thermal conduction losses from the hot flare plasma. The amount of plasma at transition region temperatures is also related to the rate of evaporation of chromospheric material into the flare loops.

In this paper we report measurements of the luminosities at transition region temperatures,  $L_{TR}$ , for several X-class flares during their impulsive phases. The measurements rely on spectra from the Ultraviolet Coronagraph Spectrometer (UVCS) of O VI photons from the flare scattered by O VI ions in the corona. Section 2 presents the UVCS observations for flares observed on 2002 July 23 and August 24, and 2003 Oct. 23, Nov. 2 and Nov. 4. We compare the results with RHESSI and GOES X-ray observations. Other aspects of the UVCS observations of the 2002 events are presented in Raymond et al. (2003), and RHESSI observations of the 23 July 2002 event are presented in a special issue of ApJ Letters (2003, ApJ Letters 595). Section 3 presents the analysis of the UVCS observations, section 4 describes the analysis of the X-ray observations, and section 5 summarizes the observed luminosities and compares the radiative losses, thermal conduction losses, energy deposition by non-thermal particles and the rate of change of thermal energy in the X-ray emitting plasma.

## 2. UVCS Observations

UVCS (Kohl et al. 1995) is a longslit UV spectrograph fed by a coronagraph. The 40' slit is placed parallel to a tangent to the solar limb at heliocentric distances between 1.5 and 10  $R_{\odot}$ . In all the cases discussed here, UVCS was performing a CME watch, taking a long series of short exposures above an active region near the limb that had been chosen for its likelihood to produce a Coronal Mass Ejection (CME). The observations presented here consist of sequences of 120 second exposures separated by about 10 second readout intervals. The UVCS slit was placed at 1.63  $R_{\odot}$ , and the 100  $\mu$  slit width provided spectral resolution of about 0.4 Å. In all cases one panel of the detector mask covered the 1024 - 1042 Å range, and other panels covered lines of ions such as C III, Si XII and [Fe XVIII]. Here we will discuss mainly the O VI lines. The line intensities were determined based on current calibration files, including the loss of sensitivity over time for narrow settings of the internal occulter based on Gardner et al. (2002).

In all five cases a CME occurred, but during the interval between the flare onset in hard X-rays and the time the CME reached the UVCS slit, the lines of O VI at 1031.9Å and 1037.6Å brightened. In all cases it is obvious when the CME reaches the UVCS slit

because of large disturbances in the Doppler widths and velocity centroids of the lines, and because O VI and other lines fade rapidly as hot, low density plasma displaces the pre-CME streamer gas.

We interpret the O VI brightening before the CME reaches the UVCS slit as radiation from the flare scattered by O VI ions in the corona. We are confident of this interpretation for several reasons: 1) The O VI brightening occurs simultaneously along the entire length of the slit, while the CME disturbance affects the center of the slit first, and the disturbance spreads along the slit over the course of several exposures (see Figure 2 of Raymond et al. 2003). 2) The additional O VI emission shows an intensity ratio  $I(1032)/I(1037)$  of approximately 4:1 (Figure 1, right panel), characteristic of scattering of solar disk O VI lines, rather than the 2:1 ratio produced by collisional excitation of O VI ions in the corona. 3) The centroids and widths of the line profiles are unchanged from their pre-CME values. 4) The O VI emission peaks coincide with the RHESSI hard X-ray peaks in the three events where the comparison can be made (Figures 1 and 2).

Figure 1 shows the intensities of the O VI 1032Å line and the RHESSI hard X-ray and GOES soft X-ray fluxes for the 2003, Nov. 4 event. The other four events are shown in Figure 2. We have summed the O VI flux along the entire UVCS slit after subtracting as background the average of about 50 pre-flare exposures. A uniform background on the UVCS detector can arise during the flare due to X-rays penetrating the front of the UVCS instrument or to energetic particles. The contributions of X-rays and energetic particles can be identified by the correlation of the background with GOES X-ray and proton fluxes, respectively, but for the present purposes it only matters that the background is very smooth on Ångstrom scales. We therefore integrate over a 1 Å band centered on the O VI  $\lambda 1032$  line and subtract as background a neighboring band centered 1.2 Å toward shorter wavelengths. For most events, the rise in background only occurs after the O VI spike we discuss here. The X-ray light curves are the GOES energy fluxes in the 0.5 to 4 and the 1 to 8 Å bands, along with the RHESSI count rates in the 50 to 100 keV band. The RHESSI observations did not cover the second O VI peak of the 2003, Nov. 4 event or the impulsive peaks of the 2002, Aug. 24 and 2003, Oct. 23 events.

For more detailed analysis we measured the intensities of the 1032 and 1037Å lines in portions of the UVCS slit large enough to provide good signal to noise, typically 8 segments. The intensities were extracted by fitting Gaussians plus continuum. Here we consider for each exposure only segments of the slit in which the line widths and shifts were unchanged from the pre-CME values. For three events we used the entire slit when possible, but after the CME disturbs the central portion we use the ends of the slit, which remain undisturbed for another 1 or 2 exposures. As seen in Figure 2 of Raymond et al. (2003), the O VI intensity near the middle of the slit drops as the CME blows away the ambient plasma, and some brightening is seen at the edges of the CME bubble. In all five events, Figures 1 and 2 show a drop in O VI intensity just after the intensity spike, because the CME removes most of the coronal plasma capable of producing or scattering O VI photons. Table 1 lists the parameters of the observations.

### 3. Analysis of the UV Observations

Several steps are required to obtain the transition region luminosity of an impulsive flare. First, we determine the O VI column density in the pre-flare corona. Then, we use that column density and the scattering cross section to determine the illuminating flux due to the flare. Finally, we use the ratio of the total radiative loss rate to the O VI emissivity to find the transition region cooling.

*Pre-CME O VI column density:* The observed O VI intensities originate from both collisional excitation in the corona and resonance scattering of O VI photons from the solar disk (Mariska, 1977; Noci, Withbroe & Kohl 1987). The collisional component has an intensity ratio  $I(1032)/I(1037) = 2:1$ , while the radiative component has a ratio of 4:1. Simple algebra yields the ratio of collisional to radiative components, and it equals

$$\frac{I_{coll}(1032)}{I_{rad}(1032)} = \frac{q_{1032}n_en_{OVI}}{n_{OVI}\sigma_{eff}WI_{disk}(1032)}, \quad (1)$$

where  $q_{1032}$  is the collisional excitation rate taken from CHIANTI (Young et al. 2003),  $n_e$  and  $n_{OVI}$  are the electron and  $O^{+5}$  densities,  $\sigma_{eff}$  is the effective scattering cross section obtained by convolving the scattering profile and the solar O VI emission profile, and  $W$  is the dilution factor averaged along the line of sight.  $W$  depends on the distribution of plasma along the line of sight, and we assume a spherically symmetric corona with density declining as  $r^{-4}$  (e.g., Gibson et al. 1999). We assume a coronal line width  $v_{1/e} = 60 \text{ km s}^{-1}$  (Kohl et al. 1997) and a solar disk emission profile width of  $30 \text{ km s}^{-1}$ . The disk O VI intensity measured by UVCS (Raymond et al. 1997),  $I_{disk}(1032)$ , was multiplied by a factor of 2 to account for the increased brightness near solar maximum and the proximity of the slit to a bright active region (Woods et al. 2005; Ko et al. 2002).

Equation 1 provides a value for  $n_e$  (e.g, Ko et al. 2002), since  $n_{OVI}$  cancels out. We then derive the O VI column density,  $N_{OVI}$ , from

$$N_{OVI} = \frac{4\pi I_{coll}(1032)}{q_{1032}n_e} \quad cm^{-2}. \quad (2)$$

*Flare O VI luminosity:* Given the O VI column density, we can derive the luminosity of the flare from the additional O VI intensity observed during the impulsive phase

$$L_{flare}(1032) = \frac{4\pi I_{flare}(1032)}{N_{OVI}\sigma'_{eff}W'} \quad photons \ s^{-1}, \quad (3)$$

where  $I_{flare}(1032)$  is the 1032 intensity spike observed by UVCS due to the flare. Note that the dilution factor  $W' = < 1/(4\pi r'^2) >$ , where  $r'$  is the distance from the flare to a point in the UVCS field of view. It differs from  $W$  in Equation 1, because the flare luminosity

originates effectively in a point source, while the pre-flare illumination arises from the solar disk. For  $W'$  we assume, as for  $W$ , a  $1/r^4$  spherical density distribution and compute the weighted average along the line of sight.

An interesting complication is that the effective scattering cross section,  $\sigma'_{eff}$ , can be affected by Doppler dimming if the flare O VI emission profile is Doppler shifted. High velocity jets, sprays or CME material will be Doppler shifted well away from the coronal absorption lines (e.g. Pike & Mason 2002; Innes et al 2001), so the UVCS O VI enhancements are insensitive to any emission from that gas. Instead, the UVCS enhancement is determined by plasma at transition region temperatures at the base of the flaring loop system. Doschek, Feldman & Rosenberg (1977) observed blue-shifts of 50-80 km s<sup>-1</sup> in transition region lines of Si IV, C IV and N V during the impulsive phase of a flare. Czakowska et al. (1999) observed a brief downflow of about 20 km s<sup>-1</sup> followed by an evaporative upflow of 50 km s<sup>-1</sup> in O V  $\lambda$ 630 in the gradual phase of a flare on 1998 Apr. 29. Milligan et al. (2006) observed a 43 km s<sup>-1</sup> downflow in O V during an explosive M-class flare. X-ray observations sometimes show upflows of several hundred km s<sup>-1</sup> (e.g. Doschek, Mariska & Sakao 1996) during the impulsive phase, and constant mass flux would suggest upflows of order 50 km s<sup>-1</sup> at transition region temperatures.

We can constrain the Doppler dimming effect, because the upflow should be directed toward the portion of the UVCS slit directly above the flare, while the ends of the UVCS slit will see only the component of the upflow velocity in that direction, or about 50% of the upflow speed. The requirement that the flare luminosity be the same for all portions of the slit then constrains the upflow speed. Figure 3 shows the derived values of the O VI luminosity as a function of position along the UVCS slit for one exposure during the 2003 Nov. 2 event for several choices of upflow speed. The luminosity must, of course, be the same all along the slit, but upflow speeds below 80 km s<sup>-1</sup> leave a dip near the middle of the slit, while a speed of 100 km/s creates a hump. We conclude that the upflow speed is about 90 km s<sup>-1</sup>. We use that value for all the exposures of this event, because the first two exposures were too noisy for a reliable determination, and in the last exposure the CME had disrupted the center of the slit, forcing us to use only the 4 bins at the ends of the slit. We find upflow speeds of 50 km s<sup>-1</sup> for the 2002, Aug. 24 and 2003, Oct. 23 events, and 90 km s<sup>-1</sup> for the 2002 July 23 and 2003 November events. From Figure 3, it can be seen that the choice of upflow speed affects the derived O VI luminosities by about a factor of 1.5 level when integrated along the slit.

*Transition Region luminosity:* We determine the emission measure (EM) of the O VI emitting gas by dividing the O VI luminosity by the emissivity from CHIANTI using the Mazzotta et al. (1998) ionization balance and Grevesse & Sauval (1998) abundances. This EM is then multiplied by a total cooling rate (Raymond, Cox & Smith 1976) modified for densities of 10<sup>12</sup> cm<sup>-3</sup> and the solar photospheric abundances of Grevesse & Sauval (1998) to obtain the power radiated from temperatures near log T = 5.5. To estimate the cooling from the transition region as a whole, we assume that the Emission Measure EM(logT) scales with temperature as appropriate for a thermal conduction boundary layer in equilibrium or an evaporative flow (Raymond & Doyle 1981), and we then multiply by the cooling rates.

For this study we define the Transition Region to be  $5.0 \leq \log T \leq 6.0$ .

Table 2 shows the derived O VI  $\lambda 1032$  luminosities and emission measures  $EM_{UV}$  (in units of  $10^{48} \text{ cm}^{-3}$ ) and the inferred power radiated at transition region temperatures,  $L_{TR}$ , along with the GOES X-ray temperatures  $T_6$  and emission measures  $EM_X$  and the effective areas of the X-ray emission from RHESSI images in units of  $10^{18} \text{ cm}^2$  (see section 4). We note that the uncertainties in the luminosities derived from the ends of the slit after the center of the slit has been disturbed by the CME should be larger than the others. However, the decline in O VI luminosity for the July 23 event shown in Table 2 is similar to the decline in C III stray light brightness shown in Figure 3 of Raymond et al. (2003), suggesting that the trend is correct. We also note that the Asplund, Grevesse & Sauval (2004) set of abundances have less oxygen and would require Emission Measures larger by 50%, and the transition region luminosity,  $L_{TR}$ , would increase by about 25%. Overall, considering the uncertainties in  $N_{OVI}$ , the Doppler dimming, and the dependence of the dilution factor on the distribution of O VI along the line of sight, we estimate that the values of  $L_{TR}$  in Table 2 are good to better than a factor of 2.

#### 4. X-ray Observations

X-ray observations were obtained from the GOES and RHESSI satellites. We used the GOES data to characterize the thermal X-ray emission and the RHESSI data to determine the non-thermal emission and the size of the emitting region.

For all the flares, we measured the effective area of the X-ray source region, which we took to be the area contained within the 50% of peak flux contour in the 12-25 keV band. During the 2002 Aug. 24 flare, RHESSI went into orbital night shortly after 00:57:00 UT, and during the 2003 October 23 flare it was only possible to obtain an image during the last UVCS exposure. For the 2003 Nov. 2 and Nov. 4 flares, we only have images for the first 2 and 3 UVCS exposures, respectively. For the 2002 July 23 flare, Holman et al. (2003) obtained thick-target fits of double-power-law electron distributions with a low-energy cutoff to the spectra above the isothermal component. The minimum nonthermal electron energy flux,  $L_{NT}$ , for each time interval was derived from those fits for that flare.

Temperatures, emission measures and total radiative losses of the thermal X-ray emitting plasma were derived from the GOES X-ray fluxes using the GOES Workbench in the Solar Software Package (e. g., D.M. Zarro and K. Tolbert 2006, <http://orpheus.nascom.nasa.gov/~zarro/idl/goes/goes.html>). We note that the recent results of White et al. (2005) using coronal abundances are incorporated into the software, in particular the effects of assuming “coronal” rather than photospheric abundances and CHIANTI (Young et al. 2003) atomic rates. The derived emission measures are therefore smaller and the total radiative losses larger than would have been derived using earlier software. For example, the emission measures for the July 23 event are about half those shown in Holman et al. (2003). Temperatures and emission measures could not be derived for the

last two UVCS exposures for the 2003 Nov. 4 flare, because the GOES data were saturated. Table 3 shows the total luminosity of the the X-ray emitting gas,  $L_{therm}$ , computed from the temperatures and emission measures from Table 2, along with the total conductive power (see section 5). Table 3 also includes the minimum nonthermal energy deposition rate,  $L_{NT}$ , for the July 23 event from Holman et al. (2003) and the rate of change of thermal energy in the X-ray emitting gas,  $dE/dt$ .

We compute  $dE/dt$  from the thermal energy content computed from the GOES spectra and RHESSI effective areas. The energy content of the thermal plasma as a function of time  $t$ , written as a function of the temperature  $T$  and emission measure  $EM$ , is

$$E_{th}(t) = 3kT(t)[EM(t)fV]^{1/2}, \quad (4)$$

where  $V$  is the volume of the plasma and  $f \leq 1$  is the volume filling factor. The maximum thermal energy content is obtained for a filling factor of 1. We estimate the values of  $V$  from the areas  $A$  of the X-ray source from Table 2 and calculate the volume to be  $V = A^{3/2}$ . The mean increase of the thermal energy was calculated for each 120 s UVCS exposure. The results are shown in the sixth column of Table 3. Negative values correspond to periods when there was a net loss of thermal energy.

We note that there are two possible contributions to  $dE/dt$ ; simply heating coronal gas from coronal to flare temperatures or heating chromospheric gas to flare temperatures in an evaporative flow that passes through the transition region temperature range. In most models, the latter dominates, in accordance with the high densities observed in flares (e.g. Feldman, Doschek & Kreplin 1982), though Feldman et al. (2004) attribute the high densities to compression of the coronal plasma.

## 5. Discussion

From Table 3 (third and fourth columns) it is apparent that the transition region luminosities are comparable to the X-ray luminosities in all cases. In general,  $L_{TR}$  is larger for the first few minutes. Then the X-ray flux becomes larger, presumably as chromospheric material is evaporated into the corona. However, as shown in Table 3, the transition region luminosity (third column) seldom exceeds 10% of the rate of change of thermal energy in the X-ray emitting plasma (column 6). Therefore, we find that heat conducted from the X-ray emitting plasma to lower temperature plasma and lost as radiation from plasma at  $5.0 \leq \log T \leq 6.0$  transition region temperatures does not dominate the energetics of the X-ray emitting plasma.

However, we have estimated the thermal energy of the flare from the X-ray temperatures and emission measures of the thermal components, along with the assumption that the volume approximately equals the emitting area  $A$  seen in the RHESSI images times a thickness of  $A^{1/2}$ . This estimate assumes a filling factor of 1. A filling factor of 0.1 would



reduce the thermal energies and their rates of change by a factor of 3. A filling factor of 0.01 would be required to make  $L_{TR}$  comparable to  $dE/dt$ . The densities derived from  $EM/A^{3/2}$  with  $f=1$  range from a  $10^{10}$  to a few times  $10^{11} \text{ cm}^{-3}$  so  $f=0.1$  to 0.01 would not require an unreasonably high density compared with the densities of order  $10^{12} \text{ cm}^{-3}$  from the models of Isobe et al. (2005) or density measurements based on X-ray line ratios (e.g. Doschek et al. 1981). Therefore, the values for  $dE/dt$  could be brought down to values comparable to the radiative losses if the filling factors are as low as 0.01, as inferred by Aschwanden & Aschwanden (2006), and we cannot rule out the possibility that the radiation losses are significant compared to the rate of change of thermal energy.

It is also important to compare the transition region luminosity with the power carried out of the X-ray emitting gas by thermal conduction. This power is deposited in cooler gas, where it must either be radiated away at transition region or lower temperatures, or else heat the gas to flare temperatures (evaporation, or  $dE/dt$  of the X-ray plasma). We estimate the conductive power as

$$P_{cond} = \kappa T^{7/2} A_{cross}/L_{1/2} = 2\kappa T^{7/2} g f' A^{1/2} \quad (5)$$

where  $\kappa$  is the Spitzer conduction coefficient,  $A_{cross}$  and  $L_{1/2}$  are the cross sectional area and half length of the loops. The factor  $g$  relates  $A_{cross}/L_{1/2}$  to the quantity  $A^{1/2}$  that we can derive from the area of the X-ray emission measurable from the RHESSI images. It scales approximately as  $(D/L)^{3/2}$ , where  $D$  is the loop diameter and  $L$  the loop length, and it depends on the angle from which the loops are viewed. For values  $L \sim 3$  to  $10 D$ ,  $g$  varies from 0.02 to 0.15. The values of  $P_{cond}$  in Table 3 assume  $g = 1$  to avoid introducing a subjective correction factor, so we expect that they are overestimated by about an order of magnitude. The factor  $f'$  is the areal filling factor of the flare loops at the chromosphere,  $f' \leq 1$ . Again, we tabulate values for  $f' = 1$  in Table 3 because  $f'$  is unknown. Table 3 compares the estimated conductive powers with radiative losses and the rate of increase of thermal energy in the X-ray emitting plasma. The predicted conductive powers greatly exceed the sum  $L_{TR} + dE/dt$ . This implies either that the conductive power is a serious overestimate or that other radiative losses are important.

The other likely important radiative loss that could balance the conductive power is  $\text{Ly}\alpha$ . We can obtain an upper limit to the  $\text{Ly}\alpha$  losses from the  $\text{Ly}\beta$  associated with the flare. In most cases no impulsive  $\text{Ly}\beta$  is detected, but a  $\text{Ly}\beta$  enhancement in the Nov. 4, 2003 event is clearly seen at a level of 0.018 the O VI enhancement. The radiative components of  $\text{Ly}\alpha$  and  $\text{Ly}\beta$  are typically in a ratio of 600:1 (e.g. Raymond et al. 2003), so the flare emission in  $\text{Ly}\alpha$  could be as much as 10 times the O VI emission. It is therefore comparable to  $L_{TR}$  and far smaller than  $P_{cond}$ .

It is also possible that thermal conduction could carry the energy to still lower temperatures, and that chromospheric emission at optical and UV wavelengths balances  $P_{cond}$ . However, Machado et al. (1990) find that all the other chromospheric emission in a flare adds to about as much emission as  $\text{Ly}\alpha$ . Moreover, thermal conduction is ineffective at

such low temperatures, and for values of  $P_{cond}$  and  $A$  from Tables 2 and 3 temperature gradients of order 100 K/m at  $2 \times 10^4$  K would be needed to carry the energy below the Ly $\alpha$  emission zone, making the chromosphere only 0.1 km thick. Strong UV and optical emission are observed with TRACE and SORCE during the impulsive phases of flares (e.g. Emslie et al. 2005), but this emission could result from direct heating by particle beams. It could also be produced by absorption of the half of the flare X-ray emission that illuminates the solar surface, but that reprocessed radiation would not help balance thermal conduction losses from the flare loops. The short duration of the optical and UV emission, the enormous temperature gradients required for thermal conduction to carry the energy, and the models that indicate that chromospheric emission is comparable to Ly $\alpha$  emission (Machado et al. 1980) lead to the conclusion that the optical/UV emission is mostly generated by particle beams impinging on the lower chromosphere and X-ray illumination. Thus the transition region and chromospheric emission are smaller than  $dE/dt$  except when  $dE/dt$  drops at the end of the impulsive phase, and radiative losses are unlikely to ever be comparable to the conductive losses shown in Table 3.

We conclude the Equation 5 greatly overestimates the conductive losses from the X-ray emitting plasma. The classical conduction formula gives results 2 to 10 times smaller than saturated thermal conduction (Balbus & McKee 1982) for the temperatures and size scales in Table 2 and densities obtained from the emission measure and volume,  $(EM/V)^{1/2}$ , so saturation of the conduction does not resolve the discrepancy. The factor  $g$  is unlikely to account for the difference, because the estimates of  $P_{cond}$  exceed the radiative loss and evaporative heating terms by two orders of magnitude in many cases. Therefore, the  $P_{cond}$  estimate is too large because  $f' \ll 1$ . That is, the area of the flare flux tubes at transition region and chromospheric heights is much smaller than the area measured from the RHESSI images. Schrijver et al. (2006) observed a flare with TRACE and other instruments. The 195 Å and 1600 Å images showed the footpoints of the loops, and the typical width was  $1.4 \times 10^8$  cm, as opposed to length scales  $A^{1/2}$  of order  $1.5 \times 10^9$  cm estimated from the RHESSI areas. Presumably, the magnetic flux tubes narrow down toward lower heights, reducing the conductive power by an order of magnitude or more.

We can also compare the  $L_{TR}$  with the rate of thermal energy increase in the X-ray emitting plasma and the rate of deposition of non-thermal energy. The luminosity at transition region temperatures is

$$L_{TR} = n^2 P A f' h \quad (6)$$

where  $n$  is the density,  $P$  is the average radiative loss rate coefficient at transition region temperatures, about  $4 \times 10^{-22}$  erg cm<sup>3</sup> s<sup>-1</sup>, and  $h$  is the thickness of the transition region. The rate of thermal energy input is

$$\frac{dE_{ev}}{dt} = \frac{3kT}{\mu} \dot{m} = 2.4 \times 10^{15} \frac{T}{1 \text{ keV}} \dot{m} \quad (7)$$

where  $k$  is the Boltzmann constant,  $\mu$  the effective atomic weight,  $\dot{m}$  is the rate of mass evaporation into the flare loops,  $T$  is the temperature of the X-ray loops and  $dE_{ev}/dT$  is the increase in thermal energy due to evaporation, as opposed to the total increase due to heating of coronal plasma. Since

$$\dot{m} = \mu n A f' v \quad (8)$$

for a flow speed  $v$  through the transition region,

$$L_{TR} = \frac{n}{10^{13}} \frac{1 \text{ keV}}{T} \frac{h}{v} \frac{dE_{ev}}{dt} \quad (9)$$

For  $L_{TR} \sim 0.1 dE/dt$  as in Table 3 and velocities of order  $100 \text{ km s}^{-1}$  as inferred from Figure 3, a region of 100 km thickness would imply a density near  $10^{12} \text{ cm}^{-3}$ .

The O VI luminosity could be generated with a conventional, but high pressure, transition region. For instance, a region with a density of  $10^{12} \text{ cm}^{-3}$  and thickness 10 km could match the typical areas and O VI luminosities in Table 2. However, much higher densities have been suggested for the temperature range where O VI forms. For the 2002 July 23 flare, Share et al. (2004) found densities of  $10^{14}$  to  $10^{15} \text{ cm}^{-3}$  at temperatures of  $2 \times 10^5$  to  $7 \times 10^5 \text{ K}$  based on the  $3\gamma/2\gamma$  ratio of positron annihilation. For the 2003 Nov. 2 flare, the RHESSI data are consistent with annihilation at chromospheric temperatures and densities, or with emission from warm, dense material at  $5 - 10 \times 10^4 \text{ K}$  (G. Share 2006, private communication). Doschek et al. (1977) obtained a density of  $10^{13} \text{ cm}^{-3}$  from transition region lines during an M-class flare, so  $10^{14} \text{ cm}^{-3}$  seems plausible for these X-class flares. For the lower end of the density range given by Share et al. and  $v = 90 \text{ km s}^{-1}$  as derived for the O VI line, the values  $L_{TR}/\dot{E}$  implied by Table 2 yield values of  $h$  of order 0.1 km. We note that equation 9 allows larger values of  $h$  if most of  $dE/dt$  is attributed to heating of coronal gas rather than evaporation. However, one would predict very small values of  $h$  from the emission measures and areas in Table 2 for the density range proposed by Share et al. (2004).

Such a small value of  $h$  seems difficult to explain with Coulomb collisions as the only mechanism that stops the beam of energetic particles impinging on the chromosphere. It seems possible that sudden deposition of energy might produce plasma turbulence, and this turbulence could help to stop the particles, further increasing the energy deposition rate in a positive feedback loop to generate heating in a very thin layer. In any case, the O VI emission detected by UVCS places a firm upper limit on the emission measure at the densities and temperatures inferred from the RHESSI observation of the 23 July, 2002 event.

Finally, for the 2003 July 23 event, Table 3 shows that the minimum energy deposition by non-thermal particles,  $L_{NT}$ , is 2 to 15 times  $dE/dt$  and another order of magnitude larger than  $L_{TR}$ . Chromospheric losses, which are a few times  $L_{TR}$ , combined with  $dE/dt$  can balance  $L_{NT}$  during several of the UVCS exposures, but fail by an order of magnitude

during the exposure beginning at 00:24 UT. Models of the flaring chromosphere by Allred et al. (2005) show that the He II  $\lambda$  304 emission and the continuum emission can substantially exceed the Ly $\alpha$  emission, particularly if the flux in the non-thermal beam is large, and this might account for the apparent difference between sources and sinks of non-thermal energy during this time period.

## 6. Summary

We have determined the radiative losses at transition region temperatures for the impulsive phases of five X-class solar flares based on UVCS measurements of O VI photons scattered from coronal O VI ions, and we have compared them with X-ray observations.  $L_{TR}$  exceeds the X-ray luminosities early in the impulsive phase, but it is small compared to the rate of thermal energy increase in the flare loops,  $dE/dt$ , unless the filling factor  $f$  is  $\sim 0.01$ , at the low end of the plausible range. Estimates of the chromospheric radiation and Ly $\alpha$  indicate that they are comparable to  $L_{TR}$ . We note that our comparison applies only to the impulsive phase of the flare and to the efficiency with which plasma is heated to X-ray emitting temperatures. On longer time scales, the hot plasma cools by both local emission and by conductive transport to lower temperatures, where it is radiated away in the EUV.

In the case of the 2002 July 23 flare,  $dE/dt$  is a significant fraction of the estimated minimum rate of energy deposition by non-thermal particles. Estimates of thermal conduction power exceed the sum of transition region and chromospheric luminosities plus  $dE/dt$ , indicating that the simple estimate of conductive power is an overestimate. This is probably due to a small filling factor of flux tube area at the solar surface. The ratios of  $L_{TR}$  to the rates of thermal energy increase indicate that the emitting region is about 100 km thick for densities of order  $10^{12} \text{ cm}^{-3}$ , though a much smaller thickness would be implied by the high densities inferred from RHESSI observations of the positron annihilation line.

This work was supported by NASA grants NAG5-12827 and NNG06GI88G to the Smithsonian Institution. It benefited from the workshop on Coronal Mass Ejections held at Elmau and at ISSI and from the SHINE workshop in Big Sky, Montana. We are grateful to the observers who issue Max Millenium major flare watches, which helped us to obtain the UVCS observations. We thank Gerry Share for many helpful comments. GDH thanks Brian Dennis and Leah Haga for help in the analysis of the X-ray data and acknowledges partial support from the RHESSI Project. We thank an anonymous referee for helpful comments.

## REFERENCES

- Allred, J.C., Hawley, S.L., Abbett, W.P., & Carlsson, M. 2005, ApJ, 630, 573
- Aschwanden, M.J., & Aschwanden, P.D. 2006, preprint

- Asplund, M., Grevesse, N., & Sauval, J. 2004, in *Cosmic Abundances as Records of Stellar Evolution and Nucleosynthesis*, *ASP Conf. Ser.*, F.N. Bash and T.C. Barnes, eds.
- Balbus, S.A., & McKee, C.F. 1982, *ApJ*, 252, 529
- Brekke, P., Rottman, G.J., Fontenla, J., & Judge, P. 1996, *ApJ*, 468, 418
- Czaykowska, A., De Pontieu, B., Alexander, D., & Rank, G. 1999, *ApJL*, 521, L75
- Doschek, G.A., Feldman, U. & Rosenberg, F.D. 1977, *ApJ*, 215, 329
- Doschek, G.A., Feldman, U., Landecker, P.B. & McKenzie, D.L. 1981, *ApJ*, 249, 372
- Doschek, G.A., Mariska, J.T., & Sakao, T. 1996, *ApJ*, 459, 823
- Emslie, A. G., et al. 2004, *JGR*, 109, A10104
- Emslie, A. G., Dennis, B. R., Holman, G. D., & Hudson, H. S. 2005, *JGR*, 110, A11103
- Feldman, U., Doschek, G.A., & Kreplin, R.W. 1982, *ApJ*, 260, 885
- Feldman, U., Dammasch, I., Landi, E. & Doschek, G.A. 2004, *ApJ*, 609, 439
- Gardner, L.D., et al. 2002, in *The Radiometric Calibration of SOHO*, eds. A. Pauluhn, M.C.E. Huber & R. von Steiger (Noordwijk; ESA), p. 161
- Gibson, S.E., Fludra, A., Bagenal, F., Biesecker, D., Del Zanna, G., & Bromage, B. 1999, *JGR*, 104, 9691
- Grevesse, N., & Sauval, A.J. 1998, in *Solar Composition from Core to Corona*, eds. C. Fröhlich, M.C.E. Huber, S.K. Solanki and R. von Steiger (Dordrecht: Kluwer), p. 161
- Holman, G. D., Sui, L., Schwartz, R. A., & Emslie, A. G. 2003, *ApJ*, 595, L97
- Innes, D.E., Curdt, W., Schwenn, R., Solanki, S., Stenborg, G. & McKenzie, D.E. 2001, *ApJL*, 549, L249
- Isobe, H., Takasaki, H., & Shibata, K. 2005, *ApJ*, 632, 1184.
- Kane, S.R., Frost, K.J., & Donnelly, R.F. 1979, *ApJ*, 234, 669
- Ko, Y.-K., Raymond, J.C., Li, J., Ciaravella, A., Michels, J., Fineschi, S. & Wu, R. 2002, *ApJ*, 578, 979
- Kohl, J.L. 1995, *Sol. Phys.* 162, 313
- Kohl, J.L. 1997, *Sol. Phys.* 175, 613
- Machado, M.E., Avrett, E.H., Vernazza, J.E. & Noyes, R.W. 1980, *ApJ*, 242, 336

- Mariska, J.T. 1977, PhD Thesis, Harvard University
- Mazzotta, P., Mazzitelli, G., Colafrancesco, S. & Vittorio, N. 1998, A&AS, 133, 403
- Milligan, R.O., Gallagher, P.T., Mathoudiakakis, M., Bloomfield, D.S., Keenan, F.P. & Schwartz, R.A. 2006, ApJL, 638, L117
- Noci, G., Kohl, J.L., & Withbroe, G.W. 1987, ApJ, 315, 706
- Pike, C.D., & Mason, H.E. 2002, Sol. Phys., 206, 359
- Raymond, J.C., Cox, D.P. & Smith, B.W. 1976, ApJ, 204, 290
- Raymond, J.C., & Doyle, J.G. 1981, ApJ, 247, 686
- Raymond, J.C., et al. 1997, Sol. Phys., 175, 645
- Raymond, J.C., Uzzo, M., Ko, Y.-K., Mancuso, S., Wu, R., Gardner, L., Kohl, J.L., Marsden, B. & Smith, P.L. 2002, ApJ, 564, 1054
- Raymond, J.C., Ciaravella, A., Dobrzycka, D., Strachan, L., Ko, Y.-K. Uzzo, M. & Raouafi, N.-E. 2003, ApJ, 597, 1106
- Schrijver, C.J., Hudson, H.S., Murphy, R.J., Share, G.H. & Tarbell, T.D. 2006, preprint
- Share, G.H., et al. 2003, ApJL, 595, L89
- Share, G.H., Murphy, R.J., Smith, D.M., Schwartz, R.A., & Lin, R.P. 2004, ApJL, 615, L172
- Veronig, A. M., Brown, J. C., Dennis, B. R., Schwartz, R. M., Sui, L., & Tolbert, A. K. 2005, ApJ, 621, 482
- White, S. M., Thomas, R. J., & Schwartz, R. A. 2005, Sol. Phys., 227, 231
- Woods, T., et al. 2004 GRL, 31, L10802
- Woods, T., et al. 2005, JGR, 110, A01312
- Young, P.R., Del Zanna, G., Landi, E., Dere, K.P., Mason, H.E. & Landini, M. 2003, ApJS, 144, 135

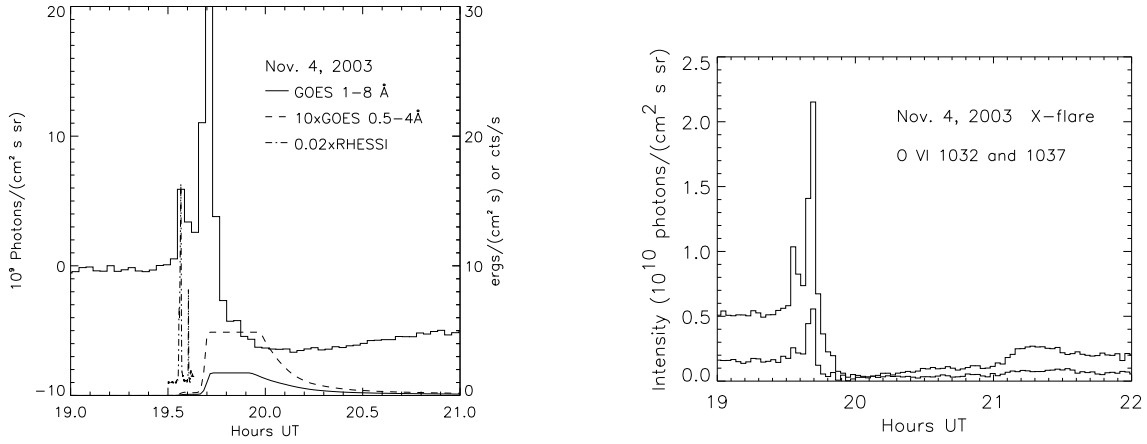


Fig. 1.— Left panel shows the O VI intensity (histogram) and X-ray fluxes for the Nov. 4, 2003 event. The pre-flare O VI intensity has been subtracted. The continuous curves show the 1–8 Å (solid) and 0.5–4 Å (dashed) GOES X-ray fluxes (right hand Y axis scale in  $\text{erg cm}^{-2} \text{s}^{-1}$ ) and RHESSI count rate (dot-dash) for photons above 50 keV (right hand axis scale in  $\text{cts s}^{-1}$ ). The flat portions of the GOES X-ray fluxes are due to saturation. Right panel shows intensities of the O VI  $\lambda\lambda$  1032 and 1037 lines as functions of time, showing the increase in the intensity ratio to approximately 4:1 during the impulsive brightening.

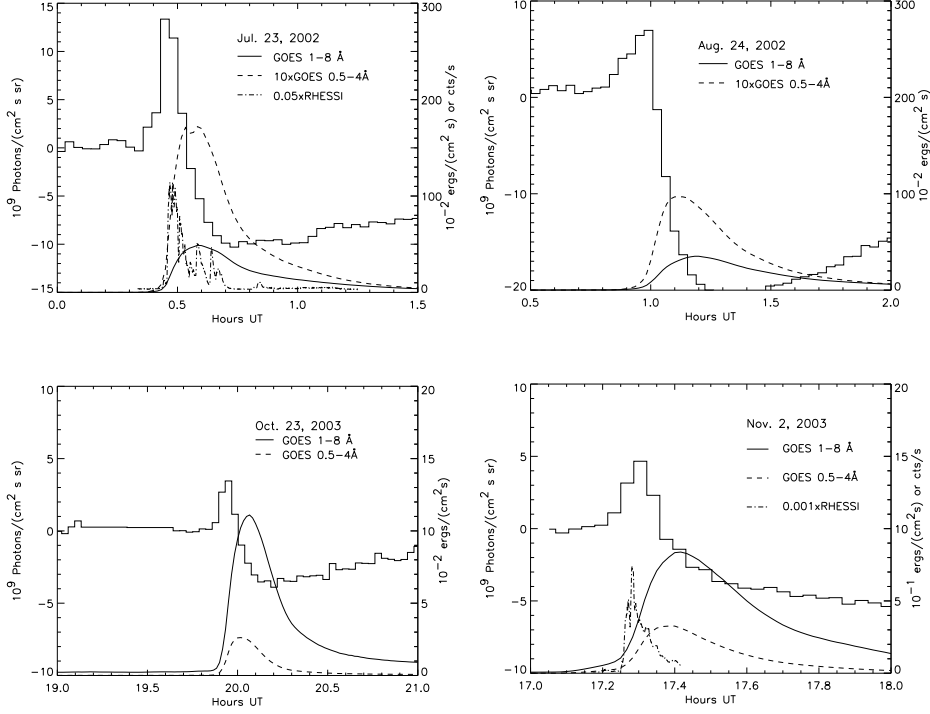


Fig. 2.— Figure 2. Time histories of the O VI  $\lambda 1032$  intensities of 4 of the events observed by UVCS (histogram). The pre-flare O VI intensity has been subtracted. The continuous curves show the 1–8 Å (solid) and 0.5–4 Å (dashed) GOES X-ray fluxes (right hand Y axis scale in  $\text{erg cm}^{-2} \text{s}^{-1}$ ) and RHESSI count rate (dot-dash) for photons above 50 keV (right hand axis scale in  $\text{cts s}^{-1}$ ).



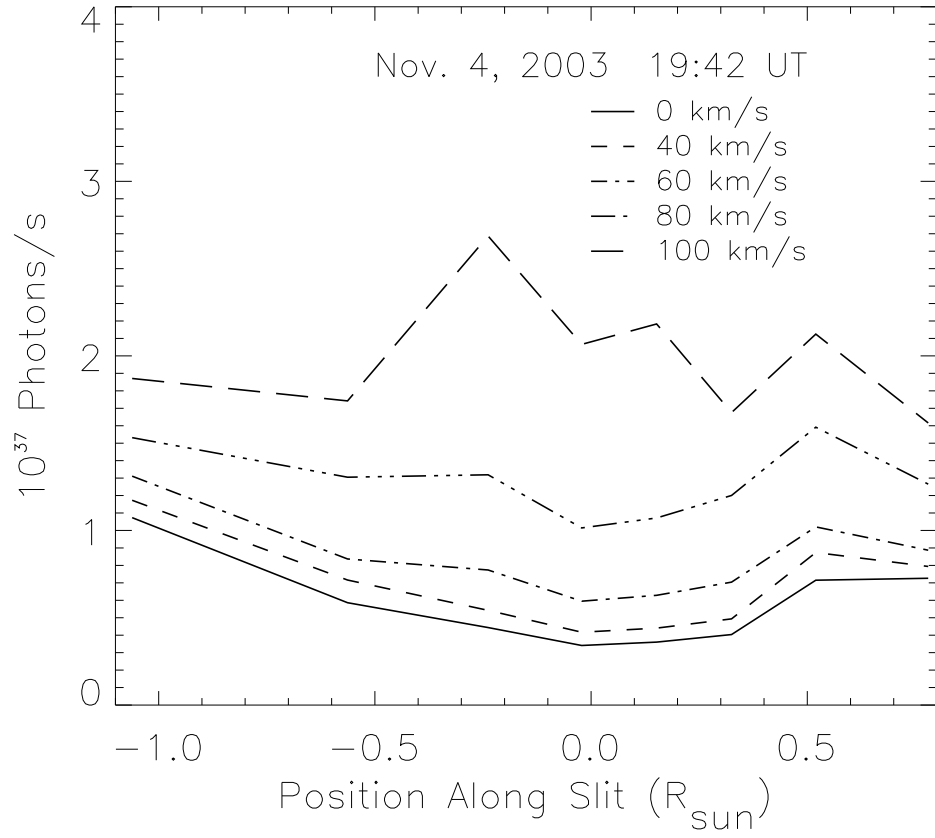


Fig. 3.— Derived O VI luminosities for different positions along the slit for the exposure beginning at 19:42 UT during the Nov. 4, 2003 event.

Table 1. UVCS Solar Flare Observations

Event	Flare Class	Flare Position	UVCS PA	Height $R_{\odot}$
Jul. 23 2002	X4.8	S13E72	96°	1.63
Aug. 24 2002	X3.1	S02W81	260°	1.63
Oct. 23 2003	X1.1	S17E84	106°	1.63
Nov. 2 2003	X8.3	S14W56	245°	1.63
Nov. 4 2003	>X28	S19W83	262°	1.63

Table 2  
Impulsive Phase O VI and X-ray Parameters  
( $10^{26} \text{ erg s}^{-1}$ ,  $10^{48} \text{ cm}^{-3}$ ,  $10^6 \text{ K}$ ,  $10^{18} \text{ cm}^2$ )

Event	$T_{\text{start}}$	$L_{1032}$	$EM_{UV}$	$L_{\text{TR}}$	$T_6$	$EM_X$	$A_{18}$
Jul. 23 2002							
	00:21:51	.19	.26	2.7	16.0	1.5	2.9
	00:24:02	.28	.39	4.0	17.5	5.8	2.8
	00:26:12	1.12	1.58	16.3	20.2	27.1	2.3
	00:28:21	.95	1.33	13.8	23.8	100.2	1.9
	00:30:32	.51	.71	7.4	22.1	171.2	2.3
	00:32:42	.28	.40	4.1	20.4	209.4	2.7
Aug. 24 2002							
	00:48:54	.03	.04	.43	12.4	0.8	26.0
	00:51:03	.06	.09	.89	14.6	1.5	18.1
	00:53:15	.13	.18	1.89	16.3	2.9	11.6
	00:55:24	.14	.20	2.03	17.6	6.3	8.9
	00:57:33	.33	.46	4.73	19.8	14.4	-
	00:59:44	.47	.66	6.82	22.2	37.5	-
Oct. 23 2003							
	19:52:16	.03	.04	.40	16.2	1.3	-
	19:54:27	.16	.23	2.33	18.8	7.7	-
	19:56:37	.20	.29	2.96	19.7	22.9	-
	19:58:46	.18	.26	2.68	18.6	39.0	0.9
Nov. 2 2003							
	17:12:37	.01	.01	.10	20.6	27.3	1.9
	17:14:48	.23	.32	3.27	21.6	51.2	10.9
	17:16:58	.43	.60	6.25	24.9	113.7	3.5
	17:19:07	.16	.22	2.29	25.8	210.6	2.6
Nov. 4 2003							
	19:31:12	.19	.27	2.7	15.5	1.6	1.5
	19:33:22	1.27	1.78	18.5	18.9	22.0	2.1
	19:35:32	.84	1.18	12.2	17.9	39.5	1.0
	19:37:45	.70	.98	10.1	16.9	42.1	-
	19:39:56	2.71	3.80	39.4	22.9	95.9	-
	19:42:06	5.32	7.47	77.5	-	-	-
	19:44:15	1.75	2.46	25.5	-	-	-

Table 3  
Radiative Losses, Thermal, Non-thermal and Conductive  
Powers ( $10^{26} \text{ erg s}^{-1}$ )

Event	$T_{\text{start}}$	$L_{TR}$	$L_{therm}$	$P_{cond}$	$dE/dt$	$L_{NT}$
Jul. 23 2002						
	00:21:51	2.7	0.7	1140	38.	156
	00:24:02	4.0	2.3	1550	72.	1240
	00:26:12	16.0	9.0	2330	228.	415
	00:28:21	13.8	29.8	3750	161.	318
	00:30:32	7.4	54.2	3180	49.	161
	00:32:42	4.1	69.3	2610	-2.	178
Aug. 24 2002						
	00:48:54	0.4	0.5	1430	39.	
	00:51:03	0.9	0.8	2090	81.	
	00:53:15	1.9	1.3	2470	77.	
	00:55:24	2.0	2.5	2830	116.	
Oct. 23 2003						
	19:58:46	2.7	14.7	1110	9.	
Nov. 2 2003						
	17:12:37	0.1	9.0	2300	41.	
	17:14:48	3.3	16.2	6400	514.	
	17:16:58	6.2	32.6	6040	347.	
	17:19:07	2.3	59.4	5810	143.	
Nov. 4 2003						
	19:31:12	2.7	0.7	749	32.	
	19:33:22	18.5	7.7	1760	155.	
	19:35:32	12.2	15.6	1015	-6.	